



**HAL**  
open science

## A robust super-resolution approach with sparsity constraint in acoustic imaging

Ning Chu, José Picheral, Ali Mohammad-Djafari

► **To cite this version:**

Ning Chu, José Picheral, Ali Mohammad-Djafari. A robust super-resolution approach with sparsity constraint in acoustic imaging. *Applied Acoustics*, 2013, pp.0000, minor revised. hal-00794236v4

**HAL Id: hal-00794236**

**<https://hal.science/hal-00794236v4>**

Submitted on 24 May 2013 (v4), last revised 29 Aug 2013 (v8)

**HAL** is a multi-disciplinary open access archive for the deposit and dissemination of scientific research documents, whether they are published or not. The documents may come from teaching and research institutions in France or abroad, or from public or private research centers.

L'archive ouverte pluridisciplinaire **HAL**, est destinée au dépôt et à la diffusion de documents scientifiques de niveau recherche, publiés ou non, émanant des établissements d'enseignement et de recherche français ou étrangers, des laboratoires publics ou privés.

# A robust super-resolution approach with sparsity constraint in acoustic imaging <sup>☆</sup>

Ning CHU<sup>a,1,\*</sup>, José PICHERAL<sup>b</sup>, Ali MOHAMMAD-DJAFARI<sup>a</sup>

<sup>a</sup>*Laboratoire des signaux et systèmes (L2S), CNRS-SUPELEC-UNIV PARIS SUD, 91192 GIF-SUR-YVETTE, FRANCE*

<sup>b</sup>*SUPELEC, Département du Signal et Systèmes Electroniques, 91192 GIF-SUR-YVETTE, FRANCE*

---

## Abstract

Acoustic imaging is a standard technique for mapping positions and powers of acoustic sources using microphone arrays, which often causes an ill-posed inverse problem. In this article, we firstly improve the forward model of acoustic power propagation by considering background noises at the sensor array, and the propagation uncertainty caused by wind tunnel effect. We then propose a robust super-resolution approach via sparsity constraint for the acoustic imaging in strong background noises. The sparsity parameter is adaptively derived from the sparse distribution of source powers. The proposed approach can jointly reconstruct source powers and positions, as well as the background noise power. Our approach is compared with the conventional beamforming, deconvolution and sparse regularization methods by simulated, real data and hybrid data respectively. It is feasible to apply our approach for mapping complex monopole sources using the 2D non-uniform microphone array in wind tunnel tests.

*Keywords:* Localization, parameter estimation, acoustic imaging, sparsity constraint, robust super-resolution

---

## 1. Introduction

Acoustic imaging is used for the acoustic source localization and power reconstruction using microphone sensors. It can provide the insights into acoustic properties, acoustic comfort and machinery security in automobile and aeronautic industries for wind tunnel tests [1–4]. In this article, we mainly focus on the signal processing techniques applied in acoustic imaging, such as the conventional beamforming, deconvolution and regularization methods, as well as our proposed approach. The conventional beamforming [5] is a direct, robust and rough estimation for acoustic imaging, since its spatial resolu-

tion is limited due to the high side-lobes. Multiple Signal Classification (MUSIC) [6] can greatly improve the conventional beamforming resolution, but original MUSIC requires the high signal-to-noise ratio (SNR) or the exact number of sources for effective subspace separation; and MUSIC could not directly reconstruct source powers due to its pseudo-power estimation. Based on the conventional beamforming, the acoustic power propagation can be modeled by a determined linear system of equations, which could hardly be solved by direct inversions. Therefore, the deconvolution methods, like the CLEAN [7], can iteratively extract strong sources from the fuzzy beamforming power image. But CLEAN could leave out weak sources interfered by strong background noises; and some important parameters of CLEAN have to be empirically selected for good performance. Recently, the Deconvolution Approach for Mapping of Acoustic Source (DAMAS) [8] has been a breakthrough and effectively applied in wind tun-

---

<sup>☆</sup>article partly based on that accepted at the IEEE International Symposium on Signal Processing and Information Technology (IS-SPIT2011) pp 286-289, Bilbao, Spain, Dec.14-17,2011.

\*Corresponding author: Ning.CHU@lss.supelec.fr. Tel. : +33 (0)1 69 85 1743. Fax : 00 33 (0)1 69 85 17 65

<sup>1</sup>The author's PhD study is financed by China Scholarship Council (CSC) and École Supérieure d'Électricité (SUPELEC) France

nel tests by the NASA. The DAMAS can iteratively solve the power propagation model under the non-negative constraint on source powers. Since the DAMAS could be sensitive to strong background noises, diagonal removal (DR)-DAMAS [8] has been proposed for the noise suppression; however, weak sources could be also removed off by the DR-DAMAS. To overcome the deconvolution drawbacks, the DAMAS with sparsity constraint (SC-DAMAS) [9] greatly improves the spatial resolution, but SC-DAMAS could be overweening to weak source detection or sensitive to strong noise interference due to the sparsity parameter selection. The Covariance Matrix Fitting (CMF) method [10] can effectively improve the robustness by jointly estimating the source power covariance matrix and background noises; however, the original CMF is not feasible to use due to its huge dimensionality of variables in covariance matrix. For robust acoustic imaging, the Spectral Estimation Method (SEM) and its extensions [11, 12] are proposed to subtract the reference noise power from the measured data for noise suppression; and this reference noise power can be obtained beforehand by measuring the observed signals without any object in wind tunnel. However, the estimated noise power might not be the same as the object exists in the wind tunnel. Furthermore, sparse regularization methods [13–15] have been widely developed by using the  $\ell_1$ -norm. However, some of them have to carefully select the regularization parameter, or make necessary approximations on subspace separation.

To summarize, all the above state-of-the-art methods have excellent performance on their own applications, but there is no one-fits-all methods; and most of them suffer one of the following drawbacks: coarse spatial resolution, sensitivity to background noises and high computational cost. In addition, most of them need to set some important parameters for good performance.

In this article, our main contributions are: we firstly improve the robust forward propagation model of acoustic power propagation by considering both the background

noises at the microphone sensors, and propagation uncertainty caused by acoustic multi-propagation effects in the wind tunnel; in order to reconstruct source powers with super-resolution and wide dynamic range, we investigate an adaptive sparsity constraint owing to the sparse distribution of source powers; and we jointly estimate source powers and positions, as well as the background noise power; for the adaptive estimation of sparsity parameter in strong background noises, we explore the incoherence of measured signal covariance matrix. Furthermore, proposed approach does not depend on parameter selection, and its computational cost maintains feasible to use.

This article is organized as follows: Section 2 briefly introduces the forward model of acoustic signal propagation. Then the improved model of acoustic power propagation is proposed in Section 3. Our proposed robust deconvolution approach with sparsity constraint is investigated in Section 4. Then we show the method performance compared with state-of-the-art methods for complex monopole source imaging through simulations in Section 5 and real data in Section 6 respectively. In order to further prove the effectiveness of proposed approach, Section 7 demonstrates the performance comparisons on the hybrid data, in which, some known synthetic sources are added to the real data. Finally we conclude this article in Section 8.

## 2. Forward model of acoustic signal propagation

### 2.1. Assumptions

For acoustic imaging, a source is usually supposed to be a uncorrelated monopole [7–9, 11, 16–18]. In this article, we use the monopole model in order to simplify the physical process and explicitly build up the forward model of acoustic propagation; to approach real cases, we use the complex monopole source which composes of several monopoles forming different spatial patterns. Moreover, we suppose that background noises are Additive Gaussian White Noise (AGWN), mutually independent and

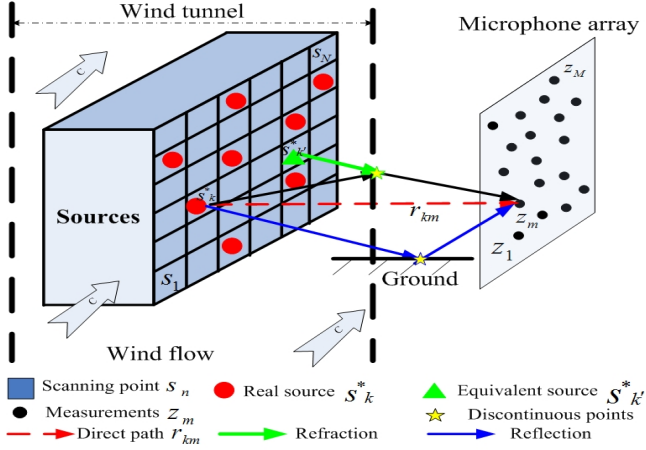


Figure 1: Illustration of acoustic propagation in the wind tunnel [19].

identically distributed (i.i.d), and independent to acoustic sources; sensors are omni-directional with unitary gain; and complex reverberations are negligible in wind tunnel, but the first order reflection at the ground and the refraction on the interface between the wind flow and common air are taken into considerations.

## 2.2. Acoustic signal propagation

Figure 1 illustrates the acoustic signal propagation from the source plane to the microphone sensor array in the open wind tunnel, where sensors are installed outside the wind flow and this causes the multi-propagation such as the ground reflection and wind refraction. We consider  $M$  sensors at the known positions on the 2D plane; and on the source plane, we suppose  $K$  unknown original source signals  $\mathbf{s}^* = [s_1^*, \dots, s_K^*]^T$  at unknown positions  $\mathbf{P}^* = [\mathbf{p}_1^*, \dots, \mathbf{p}_K^*]^T$ , where  $\mathbf{p}_k^*$  denotes the 3D coordinates of  $k$ th original source signal  $s_k^*$ ; and  $(\cdot)^T$  denotes transpose operator. In order to model the source spatial distribution, we discrete the source plane into  $N$  idetic grids at known discrete positions  $\mathbf{P} = [\mathbf{p}_1, \dots, \mathbf{p}_N]^T$ , where we assume that  $K$  original sources sparsely distribute on these grids. And we suppose  $N \gg M \gg K$  and  $\mathbf{P}^* \subset \mathbf{P}$ . Then we get  $N$  discrete source signals  $\mathbf{s}$  at known positions  $\mathbf{P}$  as follows:

$$\mathbf{s} = [0, \dots, s_1^*, 0, \dots, s_k^*, 0, \dots, s_K^*, 0, \dots]^T_N, \quad (1)$$

where  $s_k^* = s_n$  for  $\mathbf{p}_k^* = \mathbf{p}_n$ . Since  $K \ll N$ , thus  $\mathbf{s}$  is a sparse signal with  $K$ -sparsity in the spatial domain. Therefore, to reconstruct original source signals  $\mathbf{s}^*$  is transferred to reconstruct  $K$ -sparsity signals  $\mathbf{s}$ . To be clear, we state that  $\mathbf{s}^* = [s_1^*, \dots, s_K^*]^T$  denote the original source signals, while  $\mathbf{s} = [s_1, \dots, s_N]^T$  denotes the (discrete) source signals. In Eq.(1), source position  $\mathbf{p}_k^*$  can be deprived from the position  $\mathbf{p}_n$ , where the source power of  $s_n$  is not trivial.

Based on the discrete source model in Eq.(1), we can give the forward model of acoustic signal propagation. For each sensor, received signals are divided into  $I$  blocks with  $L$  samplings per block, noted as  $\mathbf{z}_{i,m}(t)$  with sensor  $m \in [1, \dots, M]$ , samplings block  $i \in [1, \dots, I]$ , sampling time  $t \in [(i-1)L + 1, \dots, iL]$  and total samplings  $T = IL$ . Since acoustic signals usually have wide-band frequencies, we apply the  $L$ -points Discrete Time Fourier Transform (DTFT) in each sampling block so as to separate the wide-band into  $L$  narrow frequency bins. Since the signal processing is made independently for each frequency bin, we omit the frequency notation  $f_l, l \in [1, \dots, L]$  at simplicity in the followings. Then the measured signals  $\mathbf{z}_i = [z_{i,1}, \dots, z_{i,M}]^T$  at the  $i$ th sampling block of all sensors can be modeled in the frequency domain as [16]:

$$\mathbf{z}_i = \mathbf{A}(\mathbf{P}) \mathbf{s}_i + \mathbf{e}_i, \quad (2)$$

where  $\mathbf{s}_i = [s_{i,1}, \dots, s_{i,N}]^T$  denotes  $N$  source signals at the  $i$ th sampling block; after DTFT,  $\mathbf{s}_i$  still maintains the sparsity in spatial domain; and  $\mathbf{e}_i = [e_{i,1}, \dots, e_{i,M}]^T$  denotes background noises at  $M$  sensors; and we suppose  $\mathbf{e}_i \sim \mathcal{N}(0, \sigma^2)$  to be the i.i.d AGWN distribution, where  $\sigma^2 = E[\mathbf{e}_i^H \mathbf{e}_i]$  denotes the noise power, with  $E[\cdot]$  denoting expectation operator and  $(\cdot)^H$  conjugate transpose; and  $M \times N$  complex matrix  $\mathbf{A}(\mathbf{P}) = [\mathbf{a}(\mathbf{p}_1), \dots, \mathbf{a}(\mathbf{p}_N)]$  denotes the signal propagation matrix, where  $\mathbf{a}(\mathbf{p}_n)$  denotes the steering vector of the source  $s_n$  at the position  $\mathbf{p}_n$  on the source plane. As shown in Fig.(1), we can improve the classical definition [16] of  $\mathbf{a}(\mathbf{p}_n)$  by modeling the first

order reflection on the ground as follows:

$$\mathbf{a}_n = \mathbf{a}_d(\mathbf{p}_n) + \rho \mathbf{a}_r(\mathbf{p}_{-n}), \quad (3)$$

where  $\rho$  denotes the reflection coefficient ( $0 \leq \rho \leq 1$ ), whose value mainly depends on ground conditions at a given frequency. For the real data used in this article,  $\rho = 0.8$  is supposed to be fixed over the frequency band [1600, 2600]Hz in the wind tunnel experiments, thanks to the research contributions of Renault SAS [20]. And  $\mathbf{a}_d(\mathbf{p}_n) = \left[ \frac{1}{r_{n,1}} e^{-j2\pi f_l \tau_{n,1}}, \dots, \frac{1}{r_{n,M}} e^{-j2\pi f_l \tau_{n,M}} \right]^T$  denotes the direct steering vector, where  $r_{n,m}$  denotes the propagation distance from source  $n$  to sensor  $m$ , and  $\tau_{n,m}$  denotes the propagation time within  $r_{n,m}$ . And  $\mathbf{a}_r(\mathbf{p}_{-n})$  denotes the reflect steering vector, similarly defined as  $\mathbf{a}_d(\mathbf{p}_n)$ , but  $\mathbf{p}_{-n}$  denotes the symmetric position to the ground of position  $\mathbf{p}_n$ . For  $r_{n,m}$  and  $\tau_{n,m}$  on the real data in Section 6, we can apply mirror sources to analyze the ground reflection, as well as use equivalent sources for the wind refraction as discussed in authors' article [19]. If not, there would be position shifts due to the wind refraction and ghost shadows due to the ground reflection.

In short, forward model of signal propagation in Eq.(2) is an under-determined linear system of equations for discrete source signals  $\mathbf{s}$  and background noises  $\mathbf{e}$ , since the measured signals  $\mathbf{z}$  are known and signal propagation matrix  $\mathbf{A}(\mathbf{P})$  can be calculated from Eq.(3) owing to the known discrete positions  $\mathbf{P}$  and known sensor positions.

### 3. Proposed forward model of power propagation

As we have stated in Introduction, acoustic imaging mainly involves the localization and reconstruction of acoustic source powers. According to the forward model of signal propagation in Eq.(2), we can estimate source signals  $\mathbf{s}$  from measured signals  $\mathbf{z}$ , then we can calculate the acoustic powers  $\mathbf{x} = [x_1, \dots, x_N]^T$  of uncorrelated sources by  $\mathbf{x} = \text{diag}[E[\mathbf{s}\mathbf{s}^H]]$ , where  $\text{diag}[\cdot]$  denotes diagonal items. However, we confront two difficulties in solving the Eq.(2): 1). equation (2) is under-determined due to the sensor

number less than discrete source number ( $M < N$ ); 2). source signals  $\mathbf{s}$  are the complex signals, which contains two kinds of unknown variables such as amplitudes and phases. In order to overcome these obstacles and improve the robustness to noises, we propose to directly build up the forward model of acoustic power propagation by considering the background noises at the sensor array, as well as the propagation uncertainty caused by the wind tunnel.

Based on the measured signals  $\mathbf{z}_i$  at sensor array in Eq.(2), a rough estimation of source powers can be directly obtained by the conventional Beamforming method [4] as:

$$y_n = \frac{E[\tilde{\mathbf{a}}_n^H \mathbf{z}_i]^2}{\|\tilde{\mathbf{a}}_n\|_2^2} \approx \frac{\tilde{\mathbf{a}}_n^H \hat{\mathbf{R}} \tilde{\mathbf{a}}_n}{\|\tilde{\mathbf{a}}_n\|_2^2}, \quad (4)$$

where  $y_n$  denotes the beamforming power at the position  $\mathbf{p}_n$  on the source plane; and  $y_n$  can be an estimated source power  $x_n$  of discrete source signal  $s_n$ ; and  $\tilde{\mathbf{a}}$  denotes the beamforming back-projection vector (spatial filter coefficients) at position  $\mathbf{p}_n$ , defined as

$$\tilde{\mathbf{a}}_n = \frac{\mathbf{a}_n}{\|\mathbf{a}_n\|_2}, \quad (5)$$

where  $\mathbf{a}_n$  is the signal propagation steering vector defined in Eq.(3);  $\|\cdot\|_2$  denotes the vector  $\ell_2$ -norm; and  $\hat{\mathbf{R}}$  denotes the estimation of measured covariance matrix, defined as

$$\hat{\mathbf{R}} = \frac{1}{I} \sum_{i=1}^I \mathbf{z}_i \mathbf{z}_i^H, \quad (6)$$

where  $\mathbf{z}_i$  denotes measured signals at the  $i$ th sampling block in Eq.(2); and  $I$  is the total number of sampling blocks. Owing to the assumptions on uncorrelated sources and AGWN noises in Section 2.1, measured covariance matrix  $\mathbf{R}$  can be modeled as

$$\mathbf{R} = \mathbb{E}\{\mathbf{z}_i \mathbf{z}_i^H\} = \sum_{n=1}^N x_n \mathbf{a}_n \mathbf{a}_n^H + \sigma^2 \mathbf{I}_M, \quad (7)$$

where  $x_n \in \mathbf{x}$  denotes the source power of  $s_n$  at position  $\mathbf{p}_n$ ; and  $\mathbf{I}_M$  denotes the  $M \times M$  identity matrix.

If the sampling number  $T$  is large enough and block number  $I \gg 1$ , we then have  $\hat{\mathbf{R}} \approx \mathbf{R}$  in Eq.(6). Therefore, in Eq.(4) we replace  $\hat{\mathbf{R}}$  by  $\mathbf{R}$  of Eq.(7); then we obtain the

improved forward model of power propagation as follows:

$$\mathbf{y} = \mathbf{C}\mathbf{x} + \sigma^2\mathbf{1}_N + \boldsymbol{\xi}, \quad (8)$$

where random variables  $\boldsymbol{\xi} = [\xi_1, \dots, \xi_N]^T$  denote the propagation uncertainty, which represents the remaining unknown effects due to the wind reflection and refraction happened at other locations rather than the ground or wind tunnel boundary; owing to  $\boldsymbol{\xi}$ , we can derive a determined linear system of equations (8) from the approximating equation (4);  $\mathbf{1}_N = [1, \dots, 1]^T_N$  is the constant;  $\mathbf{C} = [c_{n,q}]$  with  $n, q \in [1, \dots, N]$  denote power propagation matrix [8], where its item  $c_{n,q}$  is defined [19] as:

$$c_{n,q} = \frac{\|\tilde{\mathbf{a}}_n^H \mathbf{a}_q\|^2}{\|\tilde{\mathbf{a}}_n\|_2^2}, \quad (9)$$

where beamforming steering vector  $\tilde{\mathbf{a}}_n$  and signal propagation steering vector  $\mathbf{a}_n$  are defined in Eq.(5) and Eq.(3) respectively; and  $c_{n,q}$  represents the power contribution of the  $q$ th source to the  $n$ th position on the source plane. If the microphone array is ideal enough,  $c_{n,q}$  in Eq.(9) becomes the Dirac function as  $c_{n,q} = \delta_{n,q}$  with  $\delta_{n,q} = 1$  for  $n = q$ ;  $\delta_{n,q} = 0$  for  $n \neq q$ . Then we get a simple expression as  $\mathbf{y} = \mathbf{x} + \sigma^2\mathbf{1}_N + \boldsymbol{\xi}$  from Eq.(8), which reveals that the beamforming powers  $\mathbf{y}$  measured at the sensors consist of source powers  $\mathbf{x}$ , background noise power  $\sigma^2$  and the other powers of propagation uncertainty.

Compared with the signal propagation model in Eq.(2), the improved model of acoustic power propagation in Eq.(8) can profit from the determined linear system of equations for source powers  $\mathbf{x}$ ; and measured powers  $\mathbf{y}$  can be obtained by the conventional beamforming [4] in Eq.(4); power propagation matrix  $\mathbf{C}$  can be calculated from Eq.(9).

#### 4. Proposed approach with sparsity constraint

Unfortunately,  $\mathbf{C}$  is usually a singular matrix as discussed in Ref.[8] and can not be invertible. In order to jointly estimate  $\mathbf{x}$  and  $\sigma^2$  from Eq.(8), we need to bring in useful constraints on these unknown variables. Since source powers  $\mathbf{x}$  are as K-sparsity as their source signals  $\mathbf{s}$

in Eq.(1) in the spatial domain, even though source number K is unknown, we can utilize the sparse power distributions, as well as the non-negative property to reconstruct source powers  $\mathbf{x}$  and background noise power  $\sigma^2$  for robust acoustic imaging.

##### 4.1. Classical sparse regularization methods

To solve the improved forward model of power propagation in Eq.(8), sparse regularization methods [9, 10, 13–15] have been widely applied as follows:

$$\begin{cases} \hat{\mathbf{x}} = \arg \min_{(\mathbf{x})} \{ \|\mathbf{y} - \mathbf{C}\mathbf{x}\|_2^2 + \alpha \|\mathbf{x}\|_1 \} \\ \text{s.t. } \mathbf{x} \succeq 0 \end{cases}, \quad (10)$$

where the first  $\ell_2$ -norm  $\|\cdot\|_2$  represents the data fitting part; the second  $\ell_1$ -norm  $\|\cdot\|_1$  enforces the sparsity of source power distribution, and greatly improves the spatial resolutions owing to the K-sparsity of  $\mathbf{x}$ ; and  $\ell_2 + \ell_1$  optimization has been well solved by the LASSO [21] and atomic decomposition via basis pursuit [18, 22]; the third term  $\alpha$  denotes regularization parameter, which has to be tuned carefully [22–24] for good performance.

##### 4.2. Proposed sparse deconvolution approach

Compared with classical sparse regularization method in Eq.(10), we firstly improve the robustness by minimizing the propagation uncertainty  $\boldsymbol{\xi}$ , and jointly estimating the source powers  $\mathbf{x}$  and background noise power  $\sigma^2$ . To improve the spatial resolution in strong background noises, we adaptively estimate the sparsity parameter on source powers. Therefore our proposed robust super-resolution approach with sparsity constraint (SC-RDAMAS) is expressed as follows:

$$\begin{cases} (\hat{\mathbf{x}}, \hat{\sigma}^2) = \arg \min_{(\mathbf{x}, \sigma^2)} \{ \|\mathbf{y} - \mathbf{C}\mathbf{x} - \sigma^2\mathbf{1}_N\|_2^2 \} \\ \text{s.t. } \mathbf{x} \succeq 0, \quad \|\mathbf{x}\|_1 = \beta, \quad \sigma^2 \geq 0 \end{cases}, \quad (11)$$

where sparsity parameter  $\beta$  denotes the total power of uncorrelated source signals  $\mathbf{s}$ ; and  $\beta$  is defined as:

$$\beta = \sum_{k=1}^K x_k^* = \|\mathbf{x}^*\|_1 = \|\mathbf{x}\|_1 = \text{tr}[\mathbf{X}], \quad (12)$$

where  $K$  is the total number of original source signals  $\mathbf{s}^*$ ; and  $\mathbf{x}^* = \text{diag} [E[\mathbf{s}^* \mathbf{s}^{*H}]]$  denotes the original source powers;  $\mathbf{x} = \text{diag} [E[\mathbf{s} \mathbf{s}^H]]$  denotes the (discrete) source powers;  $\mathbf{X} = E[\mathbf{s} \mathbf{s}^H]$  denotes the source power covariance matrix;  $\text{tr}[\cdot]$  denotes trace operator. If  $\beta$  in Eq.(12) is modeled too large, the estimated  $\hat{\mathbf{x}}$  from Eq.(11) would be more dispersed than expected; if  $\beta$  too small, some of weak sources would be left out. Therefore the adaptive estimation of sparsity parameter  $\beta$  is an essential issue in the proposed approach.

#### 4.2.1. Adaptive estimation of sparsity parameter

To adaptively estimate sparsity parameter  $\beta$ , we firstly keep the total power unchanged during the signal propagation in Eq.(2) as follows: we normalize each column of the signal propagation matrix  $\mathbf{A}$  as discussed in Ref.[9],  $\mathbf{A}' = [\frac{\mathbf{a}_n}{\|\mathbf{a}_n\|}]$ ,  $n \in [1, \dots, N]$ , satisfying  $\text{tr}[\mathbf{A}'^H \mathbf{A}' \mathbf{X}] = \text{tr}[\mathbf{X}]$  for uncorrelated sources. In fact,  $\mathbf{A}$  reflects the amplitude attenuation after the acoustic propagation, while  $\mathbf{A}'$  reflects the amplitude compensation. According to the definition of source power covariance matrix  $\mathbf{R}$  in Eq.(7), we define  $\mathbf{R}' = \mathbf{A}' \mathbf{X} \mathbf{A}'^H + \sigma^2 \mathbf{I}_M$ ; then we can get  $\text{tr}[\mathbf{X}] = \text{tr}[\mathbf{R}'] - M\sigma^2$ . Since  $\mathbf{R}$  is also a Hermitian matrix, it can be diagonalized as  $\text{tr}[\mathbf{R}] = \text{tr}[\mathbf{U} \mathbf{\Lambda} \mathbf{U}^H] = \text{tr}[\mathbf{\Lambda}]$ , where  $\mathbf{U}$  is the unitary matrix, whose columns are eigenvectors of  $\mathbf{R}$ ; and  $\mathbf{\Lambda}$  is the eigenvalue matrix of  $\mathbf{R}$ . Finally, we can derive  $\text{tr}[\mathbf{X}] = \text{tr}[\mathbf{\Lambda}'] - M\sigma^2$ , where  $\mathbf{\Lambda}'$  is the eigenvalue matrix of  $\mathbf{R}'$ , satisfying  $\text{tr}[\mathbf{\Lambda}'] \geq \text{tr}[\mathbf{\Lambda}]$ . From the above and Eq.(12), we can obtain  $\beta$  estimation as:

$$\hat{\beta} = \text{tr}[\hat{\mathbf{\Lambda}}'] - M\hat{\sigma}^2, \quad (13)$$

where  $\hat{\mathbf{\Lambda}}'$  is obtained from measured signal covariance matrix  $\hat{\mathbf{R}}$  in Eq.(6); and  $\hat{\sigma}^2$  can be estimated as [10]:

$$\hat{\sigma}^2 = \frac{1}{M - \hat{K}} \sum_{m=\hat{K}+1}^M \hat{\lambda}_m, \quad (14)$$

where  $\hat{\lambda}_m$  denotes the eigenvalue of  $\hat{\mathbf{R}}$ , satisfying  $\hat{\lambda}_1 \geq \dots \geq \hat{\lambda}_K \geq \hat{\lambda}_{K+1} = \dots = \hat{\lambda}_M = \hat{\sigma}^2$ ; and  $M$  is the total sensor number;  $\hat{K}$  denotes the estimated source number, provided  $\hat{K} \in [0, \dots, M-1]$ . In particular case of

$\text{tr}[\mathbf{\Lambda}'] = \text{tr}[\mathbf{\Lambda}]$ , we have  $\hat{\beta} = 0$  for  $\hat{K} = 0$ ; and  $\hat{\beta} = \text{tr}[\mathbf{\Lambda}]$  for  $\hat{K} = M-1$ . Our paper [25] gives a fast and rough estimation on  $K$  as: let  $\mathcal{F}(\lambda_m)$  with  $m \in [1, \dots, M]$  denote the eigenvalue distribution function; since the big eigenvalues  $\lambda_m$  refer to original source powers  $x_k^*$  with  $k \in [1, \dots, K]$  and  $K \ll M$ , thus  $\mathcal{F}(\lambda_m)$  has a sparse distribution; and suppose  $\mathcal{F}(\lambda_m)$  to be second derivative; if its curvature  $\kappa(\lambda_{\hat{K}}) \approx 0$  at the index  $\hat{K} \in [1, \dots, M]$ , we can get the source number estimation as  $K \approx \hat{K}$  owing to the sparse distribution of  $\mathcal{F}(\lambda_m)$ . However, since the under-estimation of source number could eliminate the weak sources, it is better to initialize  $K$  as a relative big value. Therefore, we can obtain the upper bound of source number using compressed sensing [26] as:

$$K = \|\mathbf{x}\|_0 \leq \frac{1}{2} \left(1 + \frac{1}{\mu}\right), \quad (15)$$

where  $\mu = \max_{(i \neq j)} |\langle \mathbf{R}'_i, \mathbf{R}'_j \rangle|$  with  $i, j \in [1, \dots, M]$  denotes the incoherence of the measured signal covariance matrix  $\mathbf{R}'$ ; and  $\mathbf{R}'_i$  denotes the  $i$ th column. According to Eq.(7) and independence assumption between sources and noises in Section 2.1,  $\mu$  can reflect the incoherence of source power covariance matrix  $\mathbf{X}$ .

#### 4.2.2. Proposed adaptive estimation procedure

In Eq.(11), our proposed approach is a convex quadratic minimization under linear matrix constraints, which can be solved by interior point algorithms using MATLAB toolbox SeMuDi [27]. In order to improve the robustness to background noises  $\sigma^2$  and sparsity parameter  $\beta$ , we propose an adaptive estimating algorithm as depicted in Algorithm 1: Let define the cost function  $\mathcal{J}(\mathbf{x}, \sigma^2) = \|\mathbf{y} - \mathbf{C}\mathbf{x} - \sigma^2 \mathbf{1}_N\|_2^2$ ; we firstly initialize source number  $K$  by using the matrix incoherence  $\mu$  of Eq.(15); then  $\hat{\sigma}^2$  and  $\hat{\beta}$  are consequently obtained from Eq.(14) and (13); and then we simultaneously estimate source powers  $\mathbf{x}$  and  $\sigma^2$  by using the interior point algorithm [27]; finally we update  $\hat{K}^{(i+1)} = \hat{K}^{(i)} - 1$  for a new estimation.

---

**Algorithm 1** Proposed adaptive estimation procedure

---

**1. Input:**

Signal propagation matrix  $\mathbf{A}$  in Eq.(2);  
measured signal covariance matrix  $\hat{\mathbf{R}}$  in Eq.(6);  
measured beamforming powers  $\mathbf{y}$  in Eq.(4);  
power propagation matrix  $\mathbf{C}$  in Eq.(9);

**2. Initialization:**

Iteration number  $i=1$ ;  
source number  $\hat{K}^{(1)} = \frac{1}{2}(1 + \frac{1}{\mu})$  in Eq.(15);  
variables  $\hat{\mathbf{x}}^{(1)}=0$ ;  $\hat{\sigma}^{2(1)}=0$ ;  
criterion  $\mathcal{J}(\hat{\mathbf{x}}^{(1)}, \hat{\sigma}^{2(1)})=0$ ,  $\mathcal{J}(\hat{\mathbf{x}}^{(2)}, \hat{\sigma}^{2(2)})=1$ ;

**3. Iterations:**

While  $|\mathcal{J}(\hat{\mathbf{x}}^{(i+1)}, \hat{\sigma}^{2(i+1)}) - \mathcal{J}(\hat{\mathbf{x}}^{(i)}, \hat{\sigma}^{2(i)})|$  is not small enough; Else: Steps 4;

**3.1 Update:**  $\hat{\sigma}^{2(i)}$  by Eq.(14),  $\hat{\beta}^{(i)}$  by Eq.(13);

**3.2 Optimize:**

Solve Eq.(11) by interior point algorithm [27]:  
 $(\hat{\mathbf{x}}^{(i+1)}, \hat{\sigma}^{2(i+1)}) = \arg \min_{(\mathbf{x}, \sigma^2)} \left\{ \mathcal{J}(\hat{\mathbf{x}}^{(i)}, \hat{\sigma}^{2(i)}) \right\}$

s.t.  $\|\mathbf{x}\|_1 \leq \hat{\beta}^{(i)}$ ,  $\hat{\mathbf{x}}^{(i+1)} \geq 0$ ,  $\hat{\sigma}^{2(i+1)} \geq 0$ ;

**3.3 Iterate:**  $\hat{K}^{(i+1)} = \hat{K}^{(i)} - 1$ ,  $i=i+1$ ;

**4. Output:**  $\hat{\mathbf{x}}$ ,  $\hat{\sigma}^2$ ,  $\hat{K}$ ,  $\hat{\beta}$ , then **Stop**.

---

#### 4.3. Power estimation of wide-band acoustic signals

In wind tunnel tests, acoustic sources are usually generated by wind frictions against the car surface. Different car parts produce different characteristic frequencies. Therefore, acoustic signals have the wide frequency band. In Section 2, we have taken DTFT transformation and separated the wide-band into  $L$  independent frequency bins, then we have engaged incoherent signal processing at one single frequency in each frequency bin. Using the proposed SC-RDAMAS approach in Eq.(11), we can obtain  $\hat{\mathbf{x}}(f_l)$  as the estimation of source power  $\mathbf{x}(f_l)$  at  $l$ th frequency bin. Finally, total power  $\mathbf{x}_{wb}$  over the wide-band  $[f_{min}, f_{max}]$  can be estimated by averaging the summation of estimated result in each frequency bin as:  $\hat{\mathbf{x}}_{wb} = \frac{1}{L} \sum_{f_l=f_{min}}^{f_{max}} \hat{\mathbf{x}}(f_l)$ .

## 5. Simulations on uncorrelated source imaging

This section shows the typical simulations on source localization and power reconstruction of monopole sources. The proposed SC-RDAMAS approach is compared with 5 classical methods in the poor SNR cases. Reconstruction results are presented via images which can directly show the estimated source powers (dB) and positions. Then we use 3 criteria to quantitatively evaluate estimation performance. One is the averaged estimation error of original source powers, defined as  $\overline{\Delta x^*} = \frac{1}{K} \sum_{k=1}^K |\hat{x}_k^* - x_k^*|$ , where original source powers  $\mathbf{x}^* = [x_1^*, \dots, x_K^*]^T$  are defined as  $\mathbf{x}^* = \text{diag} \left[ \mathbb{E}\{\mathbf{s}^* \mathbf{s}^{*H}\} \right]$ ; the other is the reconstruction error of source power image, defined as  $\delta_2 = \frac{\|\hat{\mathbf{x}} - \mathbf{x}\|_2^2}{\|\mathbf{x}\|_2^2}$ ; compared with  $\overline{\Delta x^*}$ , the value of  $\delta_i$  not only depends on the estimated positions and powers, but also on the estimation of background noise power; the last one is the averaged position error, defined as  $\overline{\Delta p^*} = \frac{\sqrt{\sum_{k=1}^K (\mathbf{p}_k^* - \hat{\mathbf{p}}_k^*)}}{\sqrt{\sum_{k=1}^K \mathbf{p}_k^*}}$ , where  $\hat{\mathbf{p}}_k^*$  denotes the estimated positions of  $k$ th original source.

In Fig.1, simulation configurations are almost the same as the wind tunnel experiments carried out by Renault SAS [28]. For example,  $D = 4.50\text{m}$  is the distance between the sensor plane and source plane. There are  $M=64$  non-uniform sensors locating on the vertical plane. This Non-Uniform sensor Array (NUA) has a longer horizontal aperture (4m) than the vertical (2m) [28]. And it has the  $d = 3\text{m}$  averaged aperture. The advantage of NUA array is that it can yield almost the same performance but less computation burden than the uniform array with the same sensors as discussed in Ref.[29]. And  $c_0 \approx 340\text{m/s}$  is the acoustic speed in the common air.  $T = 10000$  is the total number of samplings, which is large enough to meet the important condition for the beamforming in Eq.(4) and improved forward model of power propagation in Eq.(8). To focus on method comparisons, we do not consider the ground reflection and wind refraction in simulations. But we reconsider the multi-propagation effects in wind tunnel experiments in Section 6.

For the simulated sources in Fig.2a, we have simulated



4 monopoles and 5 complex monopole sources with different patterns; and the total number of monopole sources is  $K=23$ . Sources are spaced at least 20cm. Original source powers  $\mathbf{x}^*$  are within  $[0.08,2]$   $([-10.3,3.7]\text{dB})$  and 14dB dynamic range. There are 4 parts on Fig.2a: the center image shows the source positions, patterns and powers; on its right, the colormap shows the dynamic range of source powers, in which, the dark-red colors represent strong powers, while light white colors represent the weak; on the left and bottom, 2 profile figures reveal the positions of 4 monopoles and complex monopole source on the center. To simulate the very noisy background, the noise power is set  $\sigma^2 = 0.86$  (-0.7dB), thus the averaged SNR is 0dB.

In order to make a fair comparison with other classical methods, some simulation parameters should be selected carefully. Near-field condition is guaranteed by  $D < \frac{d^2 c_0}{4f}$  for  $f > 680\text{Hz}$ . Since the spatial resolution of conventional beamforming at  $f=2500\text{Hz}$  is  $\Delta B \approx \frac{R c_0}{d f} = 31\text{cm}$ , the discrete grid is set  $\Delta p = 5\text{cm}$ , satisfying  $\frac{\Delta p}{\Delta B} < 0.2$  for any  $f < 3500\text{Hz}$ , which can avoid the spatial aliasing problem as discussed in the DAMAS [8]. For the source plane of  $100 \times 150 \text{ cm}^2$ , the power imaging is of  $21 \times 31$  pixels. Since the discrete grid number  $N = 651$  is much more larger than original source number  $K = 23$ , the discrete source signals  $\mathbf{s}$  and their source powers  $\mathbf{x}$  in Fig.2a are both  $K$ -sparsity signals.

### 5.1. Method comparisons

Firstly we show the method comparisons at 2500Hz, since this frequency is very sensitive to human hearing and affect acoustic comfort. In Fig.2, the conventional beamforming gives a fuzzy image of source power distributions; the DAMAS with 5000 iterations (5000i), CLEAN and SC-DAMAS well detect some of strong sources, but they do not provide reliable estimation of weak sources in strong background noises; the DR-DAMAS effectively removes the noise interference, but some of weak sources are also removed off; the CMF achieves better estimation on the

Table 1: Power estimations of 4 monopole sources by average power estimation error  $\overline{\Delta x^*}$ , relative errors of power image reconstruction  $\delta_2$  and estimated noise power  $\hat{\sigma}^2$  at 2500Hz, SNR=0dB, dynamic range 14dB; '-' means unavailable.

Source power	0.08	0.18	0.98	0.50	$\overline{\Delta x^*}$	$\delta_2$	$\hat{\sigma}^2$
Beamforming	1.57	11.28	3.51	2.02	69.64	121.9	-
DAMAS	-	-	-	0.44	3.14	1.33	-
CLEAN	-	0.25	0.44	0.28	0.87	0.67	-
SC-DAMAS	-	-	-	-	1.03	0.58	-
DR-DAMAS	-	-	0.77	0.23	0.30	0.08	-
CMF	0.09	-	0.80	0.40	0.31	0.10	0.89
Proposed	0.09	0.10	1.05	0.43	0.06	0.06	0.85

noise power and distinguishes most of sources; however, it fails to reconstruct some patterns of weak sources.

Table 2: Position estimations of 4 monopole sources by averaged position errors  $\overline{\Delta p^*}$  at 2500Hz, SNR=0dB; '-' means unavailable.

Source position	(-0.9,1)	(-0.6,0.75)	(-0.3,1)	(-0.6,1.3)	$\overline{\Delta p^*}$
Beamforming	-	-	-	-	1
DAMAS	-	(-0.6,0.85)	(-0.3,1)	(-0.6,1.25)	0.28
CLEAN	(-0.95,1)	(-0.6,0.75)	(-0.3,1)	(-0.6,1.3)	0.01
SC-DAMAS	-	-	-	(-0.6,1.2)	0.63
DR-DAMAS	-	-	(-0.3,1)	(-0.6,1.3)	0.43
CMF	-	(-0.6,0.9)	(-0.3,1)	(-0.6,1.3)	0.29
Proposed	(-0.9,1)	(-0.6,0.75)	(-0.3,1)	(-0.6,1.3)	0

Table 3: Power estimations of the complex monopole source on the center of image by power estimation error  $\overline{\Delta x^*}$  at 2500Hz, SNR=0dB; '-' means unavailable.

Source power	2.00	2.00	2.00	2.00	2.00	2.00	$\overline{\Delta x^*}$
Beamforming	2.64	9.60	9.70	9.64	11.34	9.77	6.78
DAMAS	4.50	1.25	0.48	2.54	0.49	1.88	1.15
CLEAN	2.29	0.37	1.69	-	0.27	0.34	1.27
SC-DAMAS	1.68	2.49	1.16	0.10	2.23	0.65	0.75
CMF	1.36	2.86	2.07	2.09	1.92	1.05	0.45
DR-DAMAS	2.15	2.05	1.82	1.83	2.50	1.45	0.27
Proposed	1.83	2.00	2.05	1.72	2.16	1.95	0.12

In Fig.2h, proposed SC-RDAMAS approach not only detects each pattern of complex monopole sources, but also well reconstructs source powers and positions in poor SNR situation. According to the 3 quantitative criteria

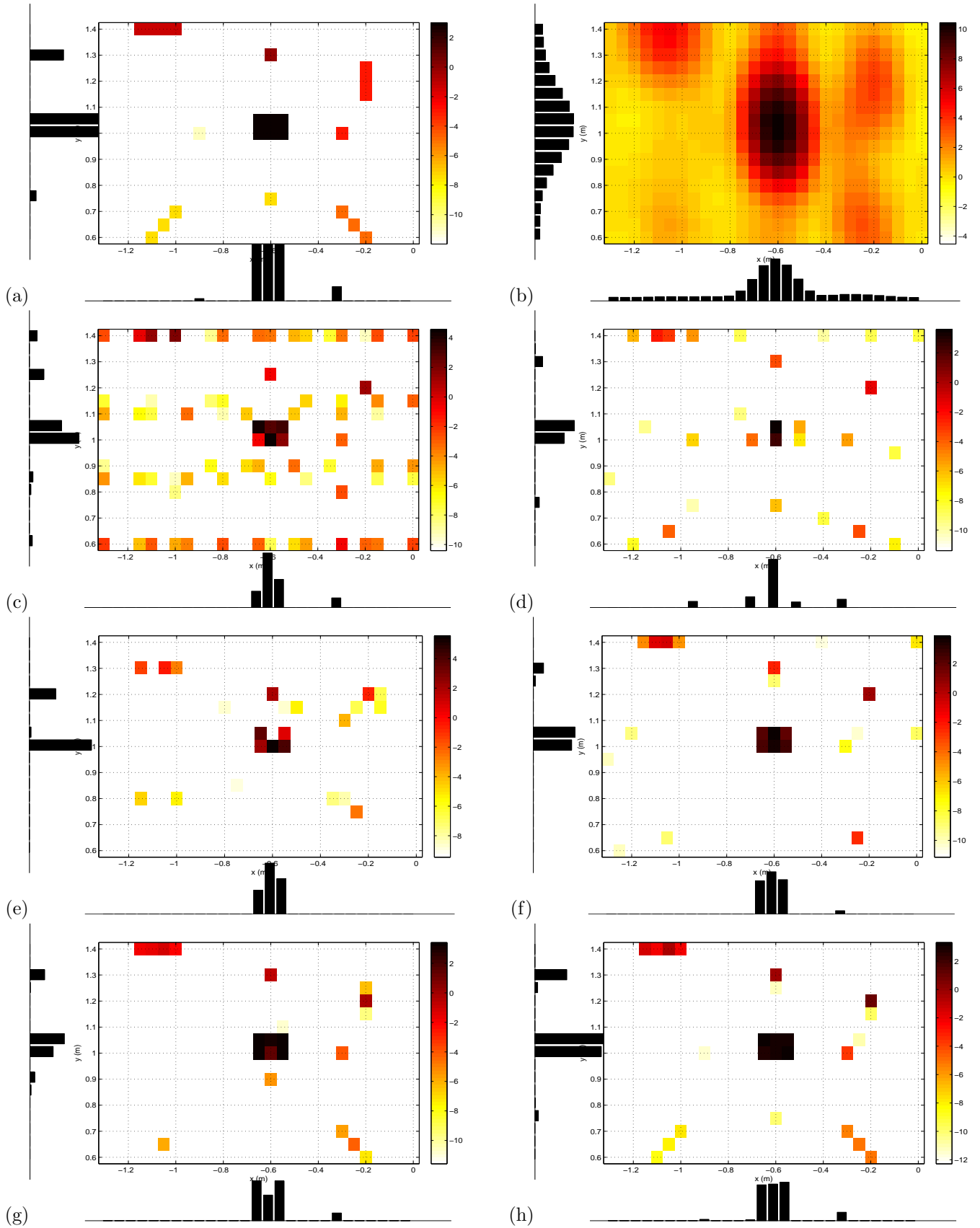


Figure 2: Simulation on monopole sources with 14dB power dynamic range at 2500Hz,  $\sigma^2 = 0.86$ , SNR=0dB and 15dB display: (a) Monopole sources (b) Beamforming (c) DAMAS with 5000 iterations (5000i) (d) CLEAN (e) SC-DAMAS (f) DR-DAMAS (5000i) (g) CMF and (h) Proposed SC-RDAMAS

$\overline{\Delta x^*}$ ,  $\overline{\Delta p^*}$  and  $\delta_2$  in the Table 1, 2 and 3, the proposed approach works much better than the others. Compared with the low spatial resolutions of conventional beamforming ( $\Delta B = 31\text{cm}$  at  $2500\text{Hz}$ ), proposed approach makes good use of sparse distribution of source powers and it achieves the resolution as high as  $5\text{cm}$  in both horizontal and vertical directions. Since the horizontal aperture of NUA array is larger than the vertical, all the results of classical methods obtain better horizontal resolution. Luckily, our proposed approach achieves the super resolution in vertical direction. Compared with the sensitiveness of deconvolution methods, proposed approach greatly improves the robustness by jointly estimating the background noise as well as the source powers. Compared with sparse regularization methods, we adaptively estimate the sparsity parameter on the total source power, so that proposed approach does not depends on parameter selection and fits well for noisy situations. Remark that CLEAN, CMF and SC-DAMAS depend on the parameter selection for better performance. To make a fair comparison, we realize the CMF, SC-DAMAS and proposed SC-RDAMAS based on Matlab toolbox SeMuDi [27].

In Fig.3, we show the relative error of power image reconstruction  $\delta_2$  of mentioned methods within SNR  $[-6, 18]\text{dB}$  at  $2500\text{Hz}$ . Proposed approach is more robust to background noises than other classical methods.

In Fig.4, we show reconstruction errors  $\delta_2$  versus different frequency bins within  $[1600, 2600]\text{Hz}$  which affects the acoustic comfort of human being. The SNR is set  $3\text{dB}$ . At high frequencies, proposed approach provides the most significant improvements. At low frequencies, proposed approach still maintains small reconstruction errors.

In Fig.5, we compare the sparsity parameter influence caused by source number estimation in the SC-DAMAS and proposed SC-RDAMAS at  $\text{SNR}=0\text{dB}$  and  $2500\text{Hz}$ . Since the complex monopole source is supposed to consist of several uncorrelated monopoles in Section 2.1, it is reasonable to take source number as  $K \in [9, 23]$  in

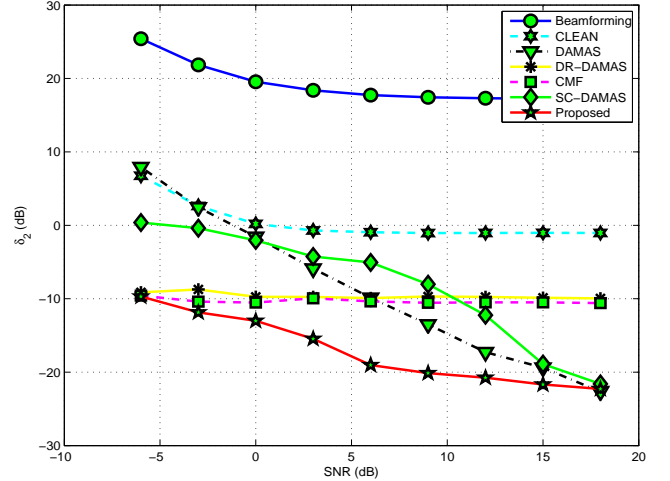


Figure 3: Performance comparison for relative errors of power image reconstruction  $\delta_2$  versus SNR  $[-6,18]\text{dB}$  on simulations at  $2500\text{Hz}$ .

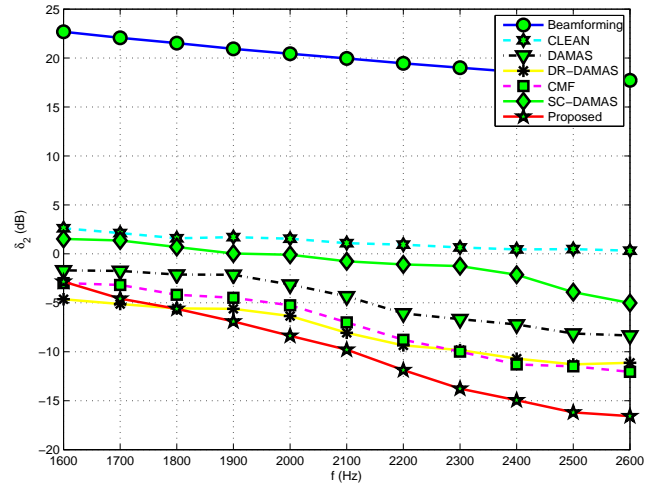


Figure 4: Performance comparison for relative errors of power image reconstruction  $\delta_2$  versus  $[1600, 2600]\text{Hz}$  on simulations at  $\text{SNR}=3\text{dB}$ .

Fig.(2)a. When source number  $\hat{K} > 23$  is over-estimated, proposed SC-RDAMAS still keeps a stable and small errors  $\delta_2$ . When under-estimated  $\hat{K} < 9$ , both the two method are very sensitive, but still our proposed approach outperforms the SC-DAMAS. On this simulation, we obtain  $\mu \approx 0.02$  from Eq.(15), then  $\hat{K}=25$  is better initialized. According to our adaptive estimation procedure in Algorithm 1, proposed SC-RDAMAS can well initialize source number  $K$  and adaptively estimate sparsity parameter  $\beta$  so as to obtain acoustic imaging with super resolution in strong background noises.

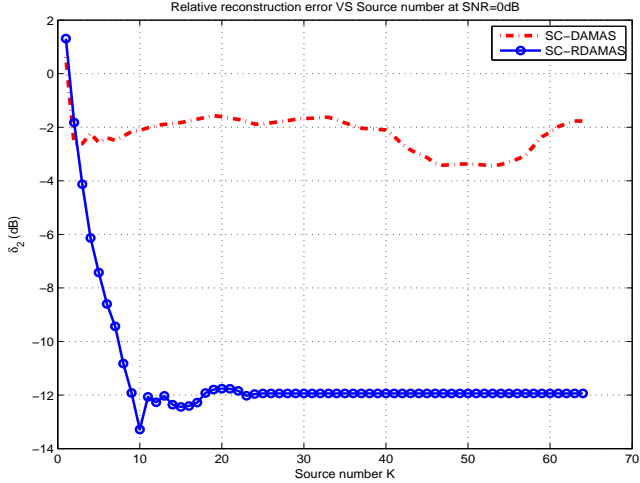


Figure 5: Sparsity parameter influence caused by estimated source number  $\hat{K}$  versus power image reconstruction error  $\delta_2$  between the SC-DAMAS and proposed SC-RDAMAS at 0dB and 2500Hz.



Figure 6: Wind tunnel S2A [28] in France.

## 6. Wind tunnel experiments

Figure 6 shows the static vehicle, microphone sensor array and the wind flow at the speed of 160km/h in the wind tunnel S2A [28]. One of objects of this wind tunnel is to detect acoustic powers and positions on the car surface. This wind tunnel can simulate a traveling car on the highway and measure its acoustic comfort to the passengers-by.

### 6.1. Experiment configurations

We suppose that all acoustic sources locate on the same plane, since the curvature of the car side is relatively small compared with the distance  $D=4.5\text{m}$  between the car and

array plane. The surface of car side is of  $150 \times 500 \text{ cm}^2$ , and we discrete this source plane into  $31 \times 101$  pixels by the discrete grid  $\Delta p = 5\text{cm}$ ; and we also focus on a small region of the rearview mirror:  $1 \times 1.5 \text{ m}^2$  ( $21 \times 31$  pixels). In the real data, there are  $T=524288$  samplings with the sampling frequency  $f_s=2.56 \times 10^4 \text{ Hz}$ . As discussed in Section 2, we separate these samplings into  $I=204$  blocks with  $L=2560$  samplings per block. The working frequency band is chosen as  $[2400, 2600]\text{Hz}$ , which is sensitive to acoustic comfort of human being. The image results are shown by normalized dB images with 10dB span. For the acoustic imaging on the vehicle surface in wind tunnel tests in Fig.(6), acoustic sources often sparsely locate on the rearview mirrors and around the wheels, while on the rest parts there are few significant sources. Therefore discrete source signals  $\mathbf{s}$  and their powers  $\mathbf{x}$  are both sparse signals. But unfortunately, we do not know the exact source number or SNR beforehand. Therefore, it is necessary to investigate the adaptive estimation procedure in Algorithm 1 for robust acoustic imaging in wind tunnel tests.

### 6.2. Results of single frequency at 2500Hz

Figure.7 illustrates the estimated power images of mentioned methods at 2500Hz. In Fig.7a, the conventional beamforming merely gives a fuzzy image of strong sources around the front wheel, rearview mirror and back wheel. In Fig.7b, DAMAS well deconvolves the beamforming image, and discovers weak sources on the front light, front cover and side window; however, many false targets are detected on the air; in Fig.7c, DR-DAMAS eliminates most of the artifacts, but it also removes off some of weak sources. Figure.7d shows that the CLEAN overcome the drawbacks of the DAMAS, but we have to carefully select the parameters for this good performance. In Fig.7e, the SC-DAMAS has a better noise suppression than the DAMAS and CLEAN owing to the sparsity parameter selection, but SC-DAMAS does not provide a wide dynamic range of source power estimations.

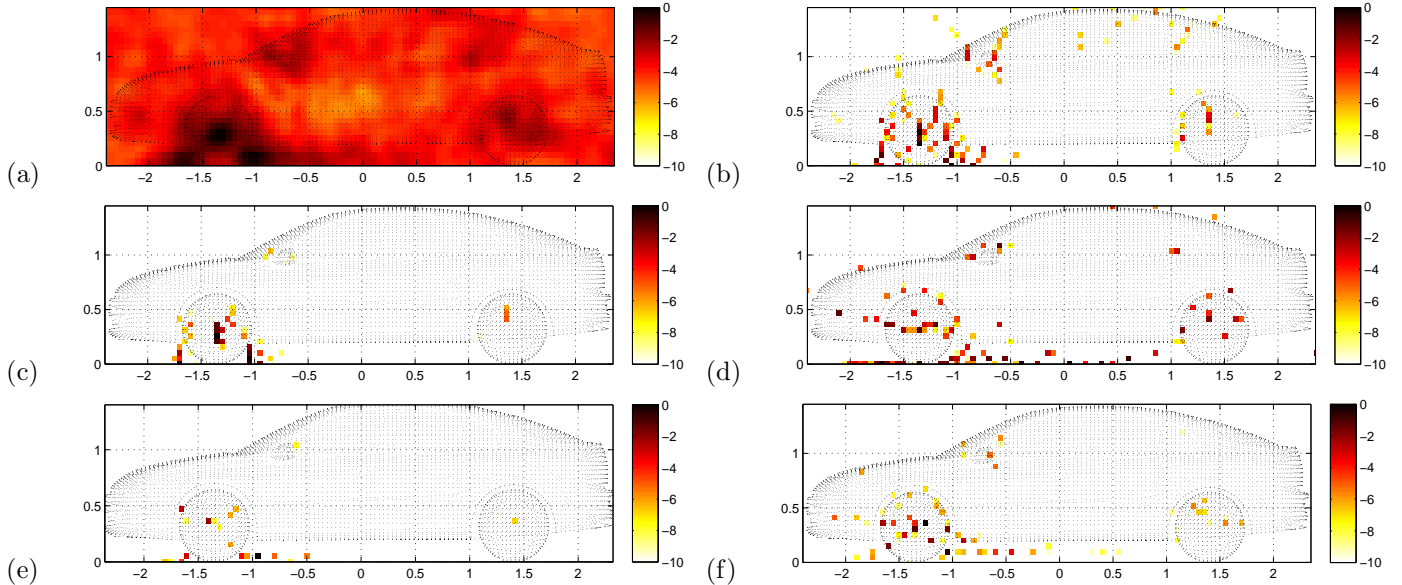


Figure 7: Acoustic imaging of real data on the whole car side at 2500Hz: (a) Beamforming (b) DAMAS (5000i) (c) DR-DAMAS (5000i) (d) CLEAN (e) SC-DAMAS and (f) Proposed SC-RDAMAS.

Table 4: Computational cost for treating whole car: image  $30 \times 100$  pixels, at 2500Hz, based on CPU:3.33GHz, '-' means unavailable.

Methods	Beamforming	DAMAS (5000i)	DR-DAMAS (5000i)	CLEAN	Proposed	SC-DAMAS	CMF
Time (s)	1	10	11	45	852	1254	Very Long

Finally in Fig.7f, proposed SC-RDAMAS not only manages to distinguish the strong sources around the two wheels, rearview mirror and side window, but also successfully reconstructs the weak ones on the front cover and light. But proposed approach could have an overweening effect caused by the sparsity constraint in compressed sensing [26] as the SC-DAMAS method, especially when the source number is under-estimated as shown in Fig.5. Moreover, the proposed adaptive estimation procedure in Algorithm 1 inevitably increases more computational cost than the deconvolution methods such as DAMAS and CLEAN; but proposed approach still remains a moderate complexity compared with sparse regularization methods such as the SC-DAMAS as shown in Table 4. Due to the high dimension of variables in source power covariance matrix, we can not realize the original CMF method in simulation.

Based on the acoustic imaging on the car side, we investigate a small part containing the rearview mirror. In

Fig.8a, conventional beamforming detects strong sources on the corner of the front wheel and rearview mirror; the DAMAS in Fig.8b improves the spatial resolutions, but it causes some unexpected spots; in Fig.8c, the DR-DAMAS eliminates most of false spots; in Fig.8e-f, the CMF, SC-DAMAS and proposed approach achieve much better resolutions and offer more detail of source power distributions on the rearview mirror.

In brief, the experiment results well agree with the simulations. The proposed SC-RDAMAS approach can achieve as good performance as the mentioned classical methods.

### 6.3. Results of wide-band data

Based on the imaging results at single frequency, we show performance comparisons of wide-band data within [2400, 2600]Hz which affects the acoustic comfort. In Fig.9, each method obtains a better result than the correspondent one at 2500Hz in Fig.7. This is because that source

powers are enforced, and the flashing false targets are suppressed over the wide-band average. The reconstruction of DAMAS in Fig.9a is acceptable, but its spatial resolution is not high enough on the front wheel and rearview mirror. Figure.9b shows that CLEAN greatly ameliorates the resolution, but unexpected points under the car caused by ground reflection should be further eliminated; the SC-DAMAS in Fig.9c has the advantages of the CLEAN, but it could not detect the weak sources around the back wheel due to the sparsity parameter selection. Finally in Fig.9d, the proposed approach provides the more accurate reconstructions of source positions and powers for the strong sources on the mirror and the front wheel, as well as weak ones on the back wheel.

## 7. Hybrid data

Even though our proposed approach obtains good performance on real data from wind tunnel experiments, it is not sufficient for method validation. This is because the exact acoustic sources on the vehicle caused by wind flow are not known beforehand. To further verify the proposed method, we use the hybrid data which composes of known synthetic sources and the real data. In order to avoid overlapping the original sources, the synthetic sources are set on the region where there are no significant sources powers. In Fig.10a, 5 synthetic complex monopole sources with different patterns are generated at 2500Hz, whose powers are within  $[-4.5, 0]$ dB. We expect that our proposed approach can detect both the synthetic and original source powers respectively from the hybrid data. If these known synthetic sources are successfully recovered, the proposed approach can be proved to effectively reconstruct the original acoustic sources on the vehicle surface. Moreover, we consider the ground reflection and wind refraction effects in both synthetic and real data.

For the synthetic sources, figure.10f shows that proposed approach successfully detects most of the source powers and patterns; for the original sources in hybrid

data, the proposed approach better discovers both strong and weak sources on two wheels and rearview mirrors, as well as obtains a better noise suppression compared with mentioned methods in Fig.10b-e.

## 8. Conclusions

In this article, we have proposed a robust super-resolution approach with sparsity constraint for robust acoustic imaging in strong background noises.

For the robustness to background noises, we have improved the forward model of power propagation by considering the noises at the sensors, as well as the propagation uncertainty caused by wind fraction and ground reflection in wind tunnel. For the super spatial resolution, we have adaptively estimated the sparsity parameter on source powers in the proposed Algorithm 1.

For the approach validation, we have presented method comparisons with classical methods. The simulations have shown that proposed approach obtained the 5cm super resolution compared with the beamforming resolution 31cm at 2500Hz; and it achieved the 15dB dynamic range of power estimations, and successfully detected complex monopole sources with different patterns. The Real data results have demonstrated that proposed approach effectively reconstructed strong sources on front wheels and rearview mirrors, as well as the weak sources on back wheels. The hybrid data experiments have furthermore proved the effectiveness for reconstructing the known synthetic sources and original sources in the real data. We have also shown the moderate computational cost of our approach for the acoustic imaging in wind tunnel tests.

For future works, it is worthwhile to investigate a hierarchical Bayesian inference with sparse priors for correlated source imaging in the colored background noises.

## Acknowledgment

The authors are deeply grateful to Dr. Jean-Luc Adam in Renault SAS for offering real data and valuable discus-

sions on our research. We thank a lot to Dr. Nicolas GAC in L2S lab for the comprehensive discussion.

## References

- [1] J. Lanslots, F. Deblauwe, K. Janssens, Selecting Sound Source Localization Techniques for Industrial Applications, *Sound and Vibration* 44 (6) (2010) 6–10.
- [2] A. B. Nagy, Aeroacoustics research in Europe: The CEAS-ASC report on 2010 highlights, *Journal of Sound and Vibration* 330 (21) (2011) 4955–4980.
- [3] M. Magalhaes, R. Tenenbaum, Sound sources reconstruction techniques: A review of their evolution and new trends, *Acta Acustica united with Acustica* 90 (2) (2004) 199–220.
- [4] J. Chen, K. Yao, R. Hudson, Source localization and beamforming, *Signal Processing Magazine, IEEE* 19 (2) (2002) 30–39.
- [5] B. Van Veen, K. Buckley, Beamforming: A versatile approach to spatial filtering, *ASSP Magazine, IEEE* 5 (2) (1988) 4–24.
- [6] R. O. Schmidt, Multiple emitter location and signal parameter estimation, *IEEE Transactions on Antennas and Propagation* 34 (1986) 276–280.
- [7] P. Sijtsma, Clean based on spatial source coherence, *International Journal of Aeroacoustics* 6 (4) (2007) 357–374.
- [8] T. Brooks, W. Humphreys, A Deconvolution Approach for the Mapping of Acoustic Sources (DAMAS) determined from phased microphone arrays, *Journal of Sound and Vibration* 294 (4-5) (2006) 856–879.
- [9] T. Yardibi, J. Li, P. Stoica, L. Cattafesta III, Sparsity constrained deconvolution approaches for acoustic source mapping, *The Journal of the Acoustical Society of America* 123(5) (May 2008) 2631–42.
- [10] T. Yardibi, J. Li, P. Stoica, N. S. Zawodny, L. N. Cattafesta, A covariance fitting approach for correlated acoustic source mapping, *Journal of The Acoustical Society of America* 127(5) (2010) 2920–2931.
- [11] D. Blacodon, Spectral estimation method for noisy data using a noise reference, *Applied Acoustics* 72 (1) (2011) 11–21.
- [12] D. Blacodon, Array processing for noisy data: Application for open and closed wind tunnels, *AIAA journal* 49 (1) (2011) 55–66.
- [13] D. Malioutov, M. Çetin, A. Willsky, A sparse signal reconstruction perspective for source localization with sensor arrays, *IEEE Transactions on Signal Processing* 53 (8) (2005) 3010–3022.
- [14] N. P. Galatsanos, A. K. Katsaggelos, Methods for choosing the regularization parameters and estimating the noise variance in image restoration and their relation, *IEEE Transactions on Image Processing* 1 (3) (1992) 332–336.
- [15] T. Suzuki, L1 generalized inverse beam-forming algorithm resolving coherent/incoherent, distributed and multipole sources, *Journal of Sound and Vibration* 330 (24) (2011) 5835 – 5851.
- [16] Y. Wang, J. Li, P. Stoica, M. Sheplak, T. Nishida, Wideband RELAX and wideband CLEAN for aeroacoustic imaging, *Journal of Acoustical Society of America* 115 (2) (2004) 757–767.
- [17] E. Sarradj, A fast signal subspace approach for the determination of absolute levels from phased microphone array measurements, *Journal of Sound and Vibration* 329 (9) (2010) 1553–1569.
- [18] P. Simard, J. Antoni, Acoustic source identification: Experimenting the l1 minimization approach, *Applied Acoustics* 74 (7) (2013) 974 – 986.
- [19] N. Chu, A. Mohammad-Djafari, J. Picheral, Robust bayesian super-resolution approach via sparsity enforcing priors for near-field wideband aeroacoustic source imaging, in: *Journal of Sound and Vibration*, Elsevier Ltd, Published, Feb. 2013. doi:doi:10.1016/j.jsv.2013.02.037.
- [20] J.-L. Adam, D. Ricot, C. Lambourg, A. Menoret, Correlated Beamforming Method for Relevant Aeroacoustic Sources Identification, in: *SAE 2009 Noise and Vibration Conference and Exhibition*, SAE, St. Charles, Illinois, United States, 19 May 2009, pp. 2009–01–2234.
- [21] R. Tibshirani, Regression shrinkage and selection via the LASSO, *Journal of the Royal Statistical Society. Series B (Methodological)* 58(1) (1996) 267–288.
- [22] S. Chen, D. Donoho, M. Saunders, Atomic decomposition by basis pursuit, *SIAM journal on scientific computing* 20 (1) (1999) 33–61.
- [23] J. Fuchs, Multipath time-delay detection and estimation, *IEEE Transactions on Signal Processing* 47 (1) (1999) 237–243.
- [24] Y. Kim, P. Nelson, Optimal regularisation for acoustic source reconstruction by inverse methods, *Journal of sound and vibration* 275 (3-5) (2004) 463–487.
- [25] N. Chu, J. Picheral, A. Mohammad-Djafari, A robust super-resolution approach with sparsity constraint for near-field wideband acoustic imaging, in: *IEEE International Symposium on Signal Processing and Information Technology*, Bilbao, Spain, Dec.14-17,2011, pp. 310–315.
- [26] E. Candes, J. Romberg, Sparsity and incoherence in compressive sampling, *Inverse problems* 23 (3) (2007) 969.
- [27] J. Sturm, Using sedumi 1.02, a matlab toolbox for optimization over symmetric cones, *Optimization methods and software* 11 (1-4) (1999) 625–653.
- [28] A. Menoret, N. Gorilliot, J.-L. Adam, Acoustic imaging in wind tunnel S2A, in: *10th Acoustics conference (ACOUSTICS2010)*, Lyon, France, 2010.
- [29] C. E. Kassis, J. Picheral, C. Mokbel, Advantages of nonuniform

**List of Figures**

1	Illustration of acoustic propagation in the wind tunnel [19]. . . . .	3
2	Simulation on monopole sources with 14dB power dynamic range at 2500Hz, $\sigma^2 = 0.86$ , SNR=0dB and 15dB display: (a) Monopole sources (b) Beamforming (c) DAMAS with 5000 iterations (5000i) (d) CLEAN (e) SC-DAMAS (f) DR-DAMAS (5000i) (g) CMF and (h) Proposed SC-RDAMAS . . . . .	9
3	Performance comparison for relative errors of power image reconstruction $\delta_2$ versus SNR [-6,18]dB on simulations at 2500Hz. . . . .	10
4	Performance comparison for relative errors of power image reconstruction $\delta_2$ versus [1600, 2600]Hz on simulations at SNR=3dB. . . . .	10
5	Sparsity parameter influence caused by estimated source number $\hat{K}$ versus power image reconstruction error $\delta_2$ between the SC-DAMAS and proposed SC-RDAMAS at 0dB and 2500Hz. . . . .	11
6	Wind tunnel S2A [28] in France. . . . .	11
7	Acoustic imaging of real data on the whole car side at 2500Hz: (a) Beamforming (b) DAMAS (5000i) (c) DR-DAMAS (5000i) (d) CLEAN (e) SC-DAMAS and (f) Proposed SC-RDAMAS. . . . .	12
8	Acoustic imaging of rearview mirror at 2500Hz: (a) Beamforming (b) DAMAS (5000i) (c) DR-DAMAS (5000i) (d) CMF (e) SC-DAMAS and (f) Proposed SC-RDAMAS . . . . .	17
9	Wide-band data over [2400,2600]Hz: (a) DAMAS (b) CLEAN (c) SC-DAMAS and (b) Proposed SC-RDAMAS . . . . .	17



10	Acoustic imaging of hybrid data on the whole car side at 2500Hz: (a) Synthetic sources (b) Beamforming (c) DAMAS (5000i) (d) CLEAN (e) SC-DAMAS and (f) Proposed SC-RDAMAS. . . . .	17
----	---	----

**List of Tables**

1	Power estimations of 4 monopole sources by average power estimation error $\overline{\Delta x^*}$ , relative errors of power image reconstruction $\delta_2$ and estimated noise power $\hat{\sigma}^2$ at 2500Hz, SNR=0dB, dynamic range 14dB; '-' means unavailable. . . . .	8
2	Position estimations of 4 monopole sources by averaged position errors $\overline{\Delta p^*}$ at 2500Hz, SNR=0dB; '-' means unavailable. . . . .	8
3	Power estimations of the complex monopole source on the center of image by power estimation error $\overline{\Delta x^*}$ at 2500Hz, SNR=0dB; '-' means unavailable. . . . .	8
4	Computational cost for treating whole car: image $30 \times 100$ pixels, at 2500Hz, based on CPU:3.33GHz, '-' means unavailable. . . . .	12

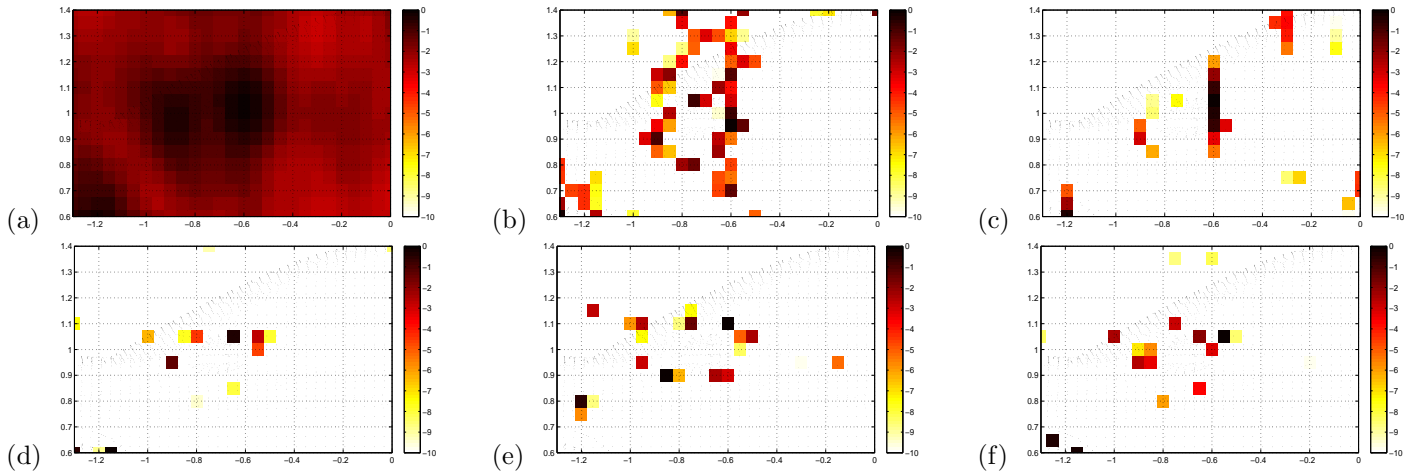


Figure 8: Acoustic imaging of rearview mirror at 2500Hz: (a) Beamforming (b) DAMAS (5000i) (c) DR-DAMAS (5000i) (d) CMF (e) SC-DAMAS and (f) Proposed SC-RDAMAS

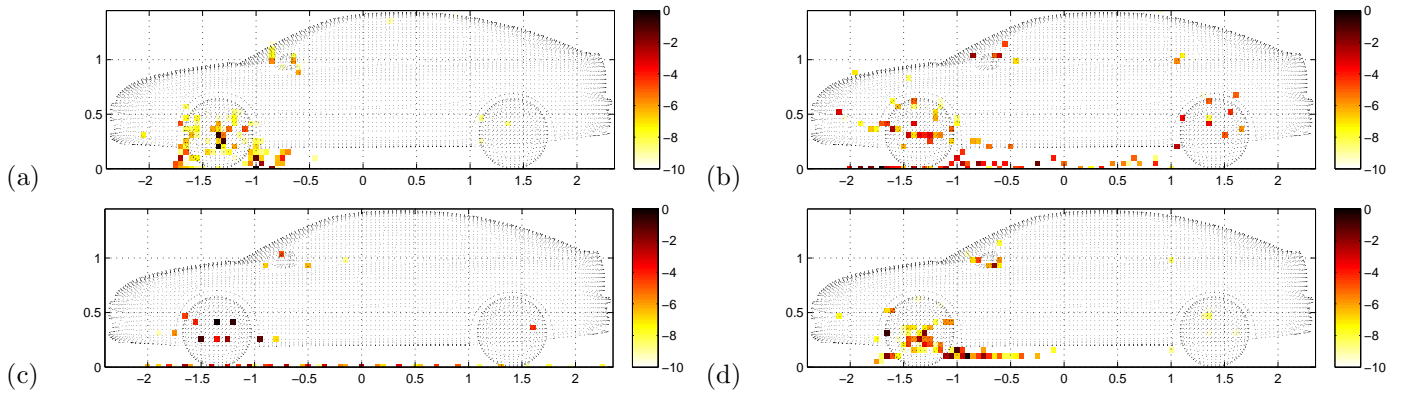


Figure 9: Wide-band data over [2400,2600]Hz: (a) DAMAS (b) CLEAN (c) SC-DAMAS and (d) Proposed SC-RDAMAS

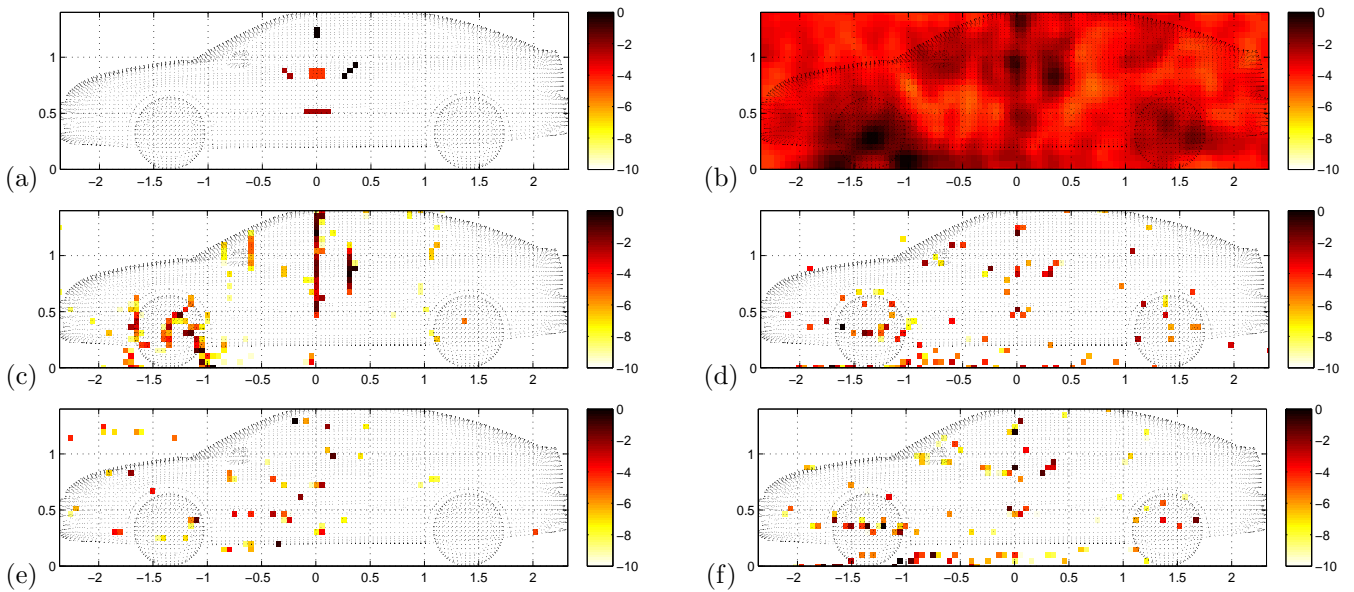


Figure 10: Acoustic imaging of hybrid data on the whole car side at 2500Hz: (a) Synthetic sources (b) Beamforming (c) DAMAS (5000i) (d) CLEAN (e) SC-DAMAS and (f) Proposed SC-RDAMAS.